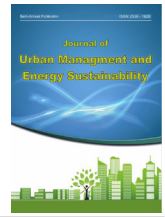
Int. J. Urban Manage. Energy Sustainability, 7(3):267-275, 2026

International Journal of Urban Management and Energy Sustainability (IJUMES)

Homepage: http://www.ijumes.com



ORIGINAL RESEARCH PAPER

Numerical Analysis of the Effect of the Soil-Cover-to-Excavation-Diameter Ratio on Surface Settlement and Ground-Strain Stability Screening of Shallow Tunnels in Clayey Soil Using PLAXIS 3D

Gholam Moradi[1*], Noora Jader Abdulhasan[2]

1 Department of Civil Engineering, University of Tabriz, Tabriz, Iran*

2 Department of Geotechnical Engineering, University of Tabriz, Tabriz, Iran

ARTICLE INFO

Article History:
Received 2026-07-11
Revised 2026-08-28
Accepted 2026-10-18

Keywords:
Clayey soil; cover-to-diameter ratio; PLAXIS 3D; shallow tunnel; surface settleme

ABSTRACT

Shallow tunnels in urban clayey ground must limit surface settlement, yet the combined influence of soil cover and excavation diameter is rarely quantified with transparent three-dimensional models. This study aims to quantify how the soil-cover-to-excavation-diameter ratio, where H is the soil cover above the tunnel crown and D is the excavation diameter, governs surface settlement and ground-strain stability of shallow tunnels in clay. Six staged-excavation models were analysed in PLAXIS 3D for D = 4.3 and 6.8 m and H/D = 0.58, 2.5 and 4.0, using a drained Mohr–Coulomb clay, a 0.30 m linear-elastic lining, 1.4 m excavation steps and case-specific face pressures of 80–100 kPa. Maximum ground strains were screened against Sakurai's critical-strain criterion, and one case was cross-checked against Peck's Gaussian trough. Crown-line surface settlement decreased monotonically with H/D, from 4.48 to 2.49 mm (44.4%) for D = 4.3 m and from 6.05 to 1.54 mm (74.5%) for D = 6.8 m. The larger diameter settled more at H/D = 0.58 and 2.5 but less at H/D = 4.0, indicating that diameter effects cannot be separated from absolute cover and face pressure. Maximum absolute ground strains ($1.03–4.88 \times 10^{-4}$) did not exceed 11% of the 4.5×10^{-3} critical strain. The Peck comparison gave a 7.42% centerline error and a mean absolute percentage error of 23.53%. H/D is therefore the dominant geometric control on settlement within the studied range, whereas ground-strain screening does not replace structural verification of segmental linings.

DOI: 10.22034/ijumes.2026.2108972.1425

Running Title: The Soil-Cover-to-Excavation-Diameter Ratio on Surface Settlement

NUMBER OF REFERENCES	NUMBER OF FIGURES	NUMBER OF TABLES
36	06	02

*Corresponding Author:
Email: *gmoradi@tabrizu.ac.ir*
Phone: 00989375120607
ORCID: https://orcid.org/0000-0002-7881-2039

INTRODUCTION

Urban tunnels provide transport and utility capacity where surface corridors are constrained, but excavation-induced movements can damage buildings, pavements, and buried services. For shallow tunnels the design problem is therefore governed by the magnitude and spatial gradient of ground settlement as well as by face-support and lining-response requirements (Loganathan & Poulos, 1998; Mair et al., 1993; Peck, 1969; Sagaseta, 1987). In this paper, shallow geometry is described by two explicit quantities: D is the excavation diameter of the circular tunnel, and H is the vertical thickness of soil cover measured from the ground surface to the tunnel crown. Their quotient H/D is called the soil-cover-to-excavation-diameter ratio. This definition is used consistently throughout the paper and must not be confused with tunnel-axis depth divided by diameter. Clayey ground can exhibit stress-history dependence, moisture sensitivity, pore-pressure effects, and nonlinear stiffness. The present archived analyses do not model all of these mechanisms: they are static, drained calculations using a Mohr–Coulomb constitutive law. Consequently, the results are interpreted as a controlled screening study rather than a complete hydro-mechanical prediction of short- and long-term clay response (Loganathan & Poulos, 1998; Mair et al., 1993; Mánica et al., 2024). The implemented lining is a continuous linear-elastic plate/shell equivalent with a nominal thickness of 0.30 m. It does not explicitly reproduce segment joints, gaskets, yielding inserts, or time-dependent grout hardening. The term flexible lining therefore refers to a future design concept and not to a yielding mechanism demonstrated by the current model; structural adequacy would additionally require axial-force, bending-moment, shear-force, joint-opening, and crack-width checks (Liu et al., 2024; Mánica et al., 2024; Mohyla et al., 2020; Suárez-Fino & Mayoral, 2024; Zaheri et al., 2020). Increasing H generally lengthens the deformation path between the excavation and the surface, whereas increasing D enlarges the excavation (Ads et al., 2021; Agarwal & Sarkar, 2024). However, H, D, face pressure, and absolute scale are coupled in the available six cases. Comparisons are therefore made within the stated parameter matrix and are not presented as a universal independent diameter effect (Chakeri et al., 2013; Chakeri & Ünver, 2014; Kasper & Meschke, 2006). The principal geometric variable is thus H/D, where H is soil cover above the crown and D is excavation diameter. Values of 0.58, 2.5, and 4.0 are evaluated for each of the two diameters. Three-dimensional staged finite-element analysis is used because the advancing face, shield activation, and progressive lining installation create longitudinal effects that cannot be represented by a plane-strain section alone. The numerical workflow is documented below through the constitutive assumptions, domain and boundary description, mesh strategy, staged excavation sequence, output variables, and empirical cross-check (Kasper & Meschke, 2006; Xie et al., 2016). The study addresses a narrow, reproducible question: how do the six archived combinations of D and H/D compare in terms of surface settlement and maximum computed ground strain under the prescribed face pressures? It does not claim a continuous optimization or complete structural design of a flexible lining. Accordingly, the objectives are to (i) quantify settlement at the reported surface points, (ii) compare the two diameter groups across H/D = 0.58, 2.5, and 4.0, (iii) screen maximum absolute ground strain against the Sakurai threshold, and (iv) report the error of an independent Peck Gaussian settlement check for one case.

MATERIALS AND METHODS

Peck (1969) formalized the Gaussian settlement-trough representation for soft-ground tunnelling. Sagaseta (1987) derived a closed-form undrained deformation field caused by near-surface ground loss. Mair et al. (1993) used field evidence from clay tunnels to describe subsurface settlement profiles, and Loganathan and Poulos (1998) introduced an analytical for-

mulation that incorporates tunnel depth, diameter, construction details, initial stress, and clay response. The width of the trough is commonly expressed as i = K·z0, where z0 is the tunnel-axis depth and K ≈ 0.4–0.5 for clays (O'Reilly & New, 1982). Kasper and Meschke (2006) used three-dimensional numerical sensitivity analyses to show that face pressure, grouting pressure, and TBM configuration materially influence ground response. Chakeri et al. (2013) compared empirical, theoretical, numerical, and observed results and identified tunnel depth, overburden, diameter, and face pressure as influential settlement variables. Chakeri and Ünver (2014) then proposed and field-checked an equation for maximum settlement above soft-ground tunnels. Fargnoli et al. (2015) back-analysed twin-tunnel construction and quantified ground and structural settlements. Xie et al. (2016) modelled a large-diameter shield tunnel in three dimensions and found that grouting pressure and execution quality can dominate surface settlement. Sharghi et al. (2017) specifically examined two-component grout properties and demonstrated their relevance to surface deformation control. Song and Marshall (2020) used centrifuge modelling to distinguish pressure-controlled and displacement-controlled tunnelling responses. Liu et al. (2021) combined field tests and finite-element analysis to show that asymmetric tail grouting alters the surface-settlement pattern. Fang et al. (2022) used centrifuge tests to demonstrate that the response of existing overlying tunnels depends on their support type, reinforcing the need to represent lining stiffness and interaction explicitly. Mohyla et al. (2020) developed a numerical approach for tunnel-lining optimisation that treats lining characteristics as design variables. Zaheri et al. (2020) compared segmental and shotcrete linings in three-dimensional shallow-tunnel faulting analyses. Mánica et al. (2024) showed that yielding support in claystone requires time-dependent constitutive representation, while Suárez-Fino and Mayoral (2024) framed lining optimisation through explicit objective functions and design variables. Liu et al. (2024) optimized a shallow-buried support system under unsymmetrical pressure and evaluated structural response rather than settlement alone. For clay-related excavation effects, Sass and Burbaum (2009) developed a test-based method for assessing adhesion of clay to tunnelling machinery and showed the sensitivity of adhesion to consistency and testing conditions. Hollmann and Thewes (2013) proposed an operational assessment framework for clay clogging and fines disintegration. These works explain excavation-operability risks, but they should not be used as substitutes for post-excavation lining verification. More recently, Ads et al. (2021) used transparent-soil models of soft clay with three cover-to-diameter ratios and showed that arching above the crown diminishes gradually as the ratio increases, while Agarwal and Sarkar (2024) reported, in a PLAXIS 2D parametric study of layered ground, that increasing the tunnel-axis depth from 10 to 30 m at a fixed 6.5 m diameter reduced the maximum surface settlement by about 63% and widened the trough. Neither study combined two excavation diameters at identical H/D values in a staged three-dimensional model or reported the empirical validation error together with a critical-strain screen.

The literature therefore supports direct assessment of settlement, face and grout pressures, soil-lining interaction, and structural lining actions. The research gap addressed here is therefore the lack of a transparent three-dimensional comparison in which the same H/D values are applied to two excavation diameters and the resulting settlements are reported together with a critical-strain screen and a quantified empirical validation error. The present study contributes only a six-case PLAXIS 3D screening of settlement and ground strain. Its scope is deliberately separated from continuous lining optimisation, time-dependent clay behaviour, and full segment-joint design .

Methodology

Scope and response variables

Six static, drained PLAXIS 3D cases were evaluated. The primary response is vertical surface settlement at points A–E; point A is located above the tunnel axis. Maximum computed ground strain is used only for Sakurai screening. Lining axial force, bending moment, shear, joint rotation, joint opening, and crack width were not archived and therefore are not claimed as verified outputs.

Geometry and parameter definitions and Soil and lining constitutive models

D denotes the circular excavation diameter (4.3 or 6.8 m). H denotes the vertical soil cover from the ground surface to the tunnel crown. The dimensionless ratio H/D takes values 0.58, 2.5, and 4.0 for each diameter. The nominal lining thickness is 0.30 m. Prescribed face pressures are 80 kPa for the (D, H/D) combinations (4.3 m, 0.58) and (6.8 m, 0.58); 90 kPa for (4.3 m, 2.5), (4.3 m, 4.0), and (6.8 m, 2.5); and 100 kPa for (6.8 m, 4.0). Face pressure is therefore a case-specific input, not an independently optimized variable. The clay layer is represented by a drained Mohr–Coulomb model as implemented in PLAXIS 3D (Bentley Systems, 2024) with E = 30,000 kN/m², cohesion c = 45 kN/m², friction angle φ = 25 degrees, Poisson ratio ν = 0.25, unsaturated unit weight 17 kN/m³, and saturated unit weight 20 kN/m³. Initial stresses use the normally consolidated K_0 procedure, $K_0 = 1 - \sin(\varphi)$. This simple model does not capture small-strain stiffness, stress-history dependence, anisotropy, creep, or consolidation.

The 0.30 m concrete lining is represented by a continuous linear-elastic plate/shell equivalent with E = 31.4 GPa, ν = 0.15, and unit weight 24 kN/m³, corresponding to axial and bending stiffnesses of EA = 9.42×10^6 kN/m and EI = 7.07×10^4 kN·m²/m per metre run. Segment joints, gaskets, local contact opening, yielding devices, and grout hardening are absent. Accordingly, the computed response is that of an equivalent continuous lining and cannot demonstrate the mechanisms of a segmented or yielding flexible system.

Domain, boundary conditions, and mesh

The archived model descriptions report horizontal domains of 60 m × 20 m for the D = 4.3 m group and 70 m × 40 m for the D = 6.8 m group. Normal displacement is restrained on the vertical side boundaries, the base is fixed in all translational directions, and the ground surface is free. The exact vertical domain extent is not available in the archived manuscript, so residual boundary influence cannot be quantified and is retained as a limitation. (Fig. 1)

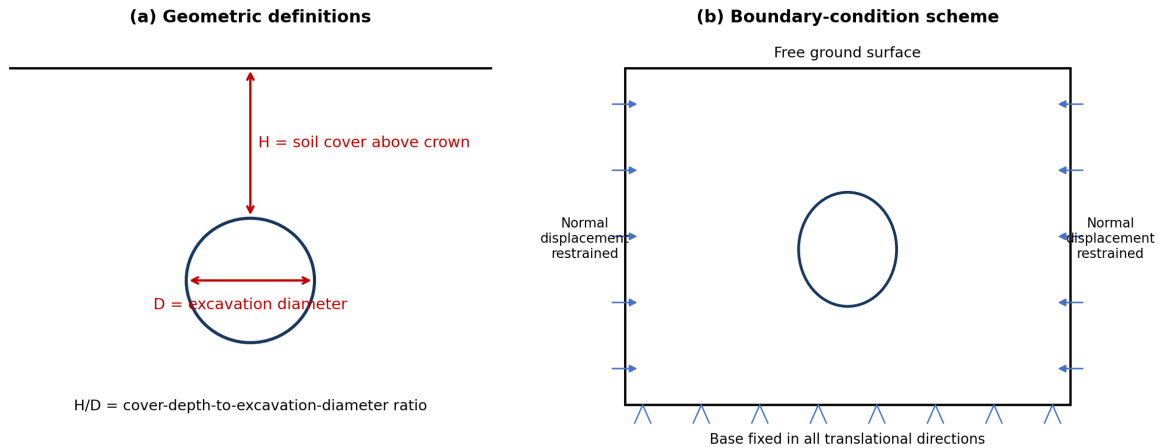


Figure 1: Definition of H and D and the adopted boundary-condition scheme

The three-dimensional soil domain is discretized with volume elements, while the shield and lining use structural plate/shell elements. The mesh is locally refined around the crown, springlines, invert, and excavation face and becomes coarser toward remote boundaries. A formal coarse-medium-fine convergence dataset was not archived. Mesh-induced uncertainty is therefore acknowledged; a complete verification would require less than 5% change in crown settlement and maximum ground strain between the medium and fine meshes. (Fig. 2)

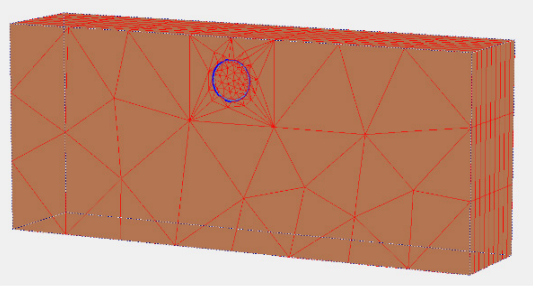


Figure 2: Archived locally refined three-dimensional mesh around the tunnel

Staged excavation and loading

The excavation advances in 1.4 m stages. In each phase the next soil slice is deactivated, the shield advances, the prescribed face pressure is transferred to the new face, and the lining is activated behind the shield following the archived phase sequence. Tail-grout injection and grout hardening were not independently parameterized; immediate lining activation is an idealization. (Fig. 3)

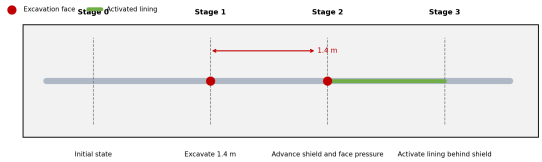


Figure 3: Schematic of the staged 1.4 m excavation, shield advance, face-pressure transfer, and lining activation

Stability screen and empirical cross-validation

The PLAXIS output labels report maximum strain in × 10^{-3} percent. Values are divided by 100 to convert percent to absolute strain before comparison with the Sakurai critical strain of 4.5 × 10^{-3} (Sakurai, 1997), defined as the ratio of uniaxial compressive strength to Young's modulus. Separately, the D = 4.3 m, H/D = 4.0 case is compared with Peck's (1969) Gaussian trough, $S(x) = S_{max} \cdot \exp(-x^2/2i^2)$, at x = 0 and ±5.5 m using pointwise absolute relative error, mean absolute error, root mean square error, and mean absolute percentage error. The reported Peck values correspond to i ≈ 8.6 m, i.e. K = i/z0 ≈ 0.44 for z0 = 19.35 m, within the range adopted for clays (O'Reilly & New, 1982), and to a volume loss of approximately 0.40%.

FINDINGS AND DISCUSSION

Surface-settlement response

At point A above the tunnel axis, settlement decreases monotonically with H/D within each diameter group. For D = 4.3 m, settlement is 4.48, 2.91, and 2.49 mm at H/D = 0.58, 2.5, and 4.0. For D = 6.8 m, the corresponding values are 6.05, 3.14, and 1.54 mm. The decrease from H/D = 0.58 to 4.0 is 44.4% for D = 4.3 m and 74.5% for D = 6.8 m. These reductions bracket the approximately 63% reduction reported by Agarwal and Sarkar (2024) when the tunnel-axis depth was tripled at constant diameter, which supports the plausibility of the computed trend. The diameter comparison is not monotonic across all equal H/D pairs: the 6.8 m case gives larger settlement at H/D = 0.58 and 2.5, but smaller settlement at H/D = 4.0. Because absolute cover and face pressure also change, the data do not isolate an independent diameter law. They support only the stated six-case comparison. (Fig. 4 and Tab.1)

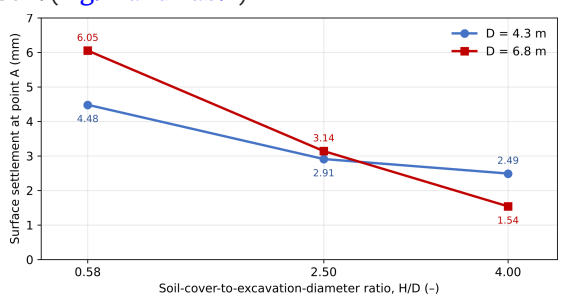


Figure 4: Crown-line surface settlement at point A for the six numerical cases (H/D plotted on a proportional axis)

Table 1: Numerical cases defined by excavation diameter D and soil cover H

Excavation diameter, D (m)	Soil cover above tunnel crown, H (m)	Soil-cover-to-excavation-diameter ratio, H/D	Face pressure (kPa)	Software
4.3	2.494	0.58	80	PLAXIS 3D
4.3	10.75	2.5	90	PLAXIS 3D
4.3	17.2	4.0	90	PLAXIS 3D
6.8	4.988	0.58	80	PLAXIS 3D
6.8	21.5	2.5	90	PLAXIS 3D
6.8	34.4	4.0	100	PLAXIS 3D

Ground-strain screening

The reported maximum strain labels are 31.73, 25.28, 25.23, 48.76, 31.49, and 10.32 × 10^{-3} percent for the six cases in Table 1 order. After conversion to absolute strain, these become 3.173 × 10^{-4}, 2.528 × 10^{-4}, 2.523 × 10^{-4}, 4.876 × 10^{-4}, 3.149 × 10^{-4}, and 1.032 × 10^{-4}. All are below the Sakurai threshold of 4.5 × 10^{-3}. This result screens ground strain only; it does not establish structural adequacy of the lining. The largest value, obtained for D = 6.8 m and H/D = 0.58, corresponds to 10.8% of the critical strain. (Fig. 5)

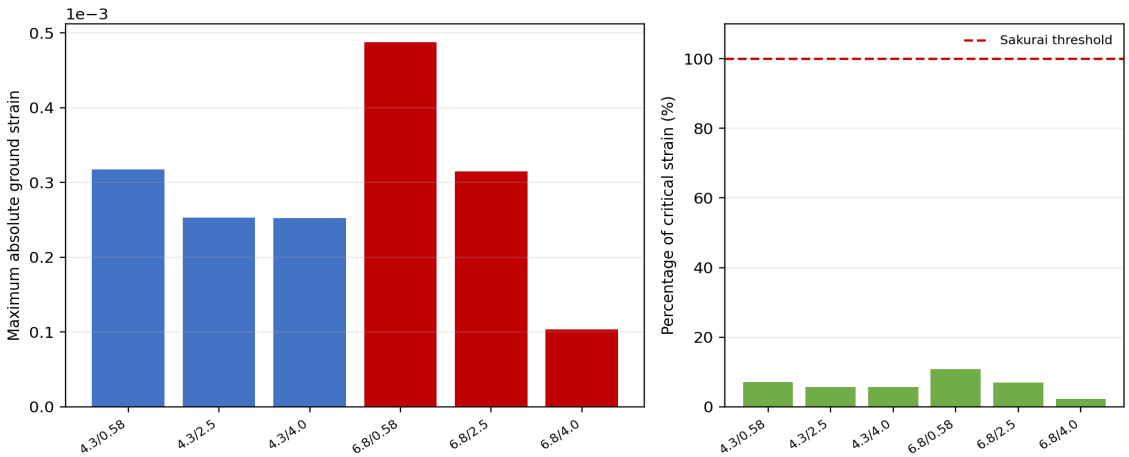


Figure 5: Maximum absolute ground strain and percentage of the Sakurai critical strain

Empirical cross-validation

For the D = 4.3 m and H/D = 4.0 case, the Peck Gaussian estimates at offsets 0, +5.5, and -5.5 m are 2.6918, 2.1939, and 2.1939 mm, while the PLAXIS values are 2.492, 1.361, and 1.641 mm. The absolute relative errors are 7.42%, 37.97%, and 25.20%, respectively; MAE = 0.529 mm, RMSE = 0.589 mm, and MAPE = 23.53%. Agreement is therefore acceptable at the centerline for screening, but weaker off axis. The difference between the PLAXIS values at +5.5 and −5.5 m (1.361 versus 1.641 mm) in a geometrically symmetric problem indicates mesh or extraction-location sensitivity and is treated as part of the numerical uncertainty. (Tab. 2 and Fig. 6)

Table 2: Pointwise Peck-versus-PLAXIS validation for the D = 4.3 m, H/D = 4.0 case

Offset x (m)	Peck estimate (mm)	PLAXIS 3D (mm)	Absolute relative error (%)
0	2.6918	2.492	7.42
+5.5	2.1939	1.361	37.97

-5.5	2.1939	1.641	25.20

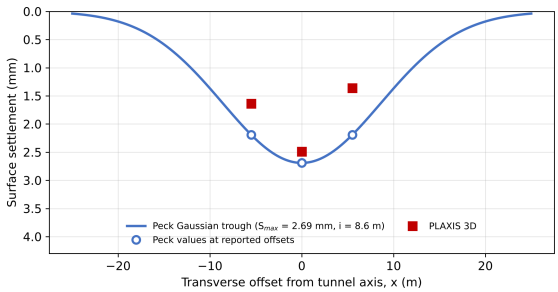


Figure 6: Peck Gaussian settlement trough (i ≈ 8.6 m) and PLAXIS 3D values at the three reported points

RESULTS AND CONCLUSION

The strongest evidence is the within-diameter reduction of point-A settlement as H/D increases. The larger-diameter cases do not consistently settle more at equal H/D, so diameter cannot be separated from absolute cover, prescribed face pressure, and the scale of the numerical domain. Likewise, the Mohr–Coulomb soil and continuous linear-elastic lining provide a screening model rather than a high-fidelity representation of clay stress history, small-strain stiffness, jointed segment behavior, or grout hardening. The principal uncertainties are the unarchived vertical boundary extent, absence of a three-level mesh-convergence dataset, and validation at only three points for one case. Future work should repeat all cases with Hardening Soil and HSsmall models, explicit groundwater and consolidation, calibrated tail-grout behavior, segment joints, extraction of M-N-V actions, and field or centrifuge measurements, together with a fully factorial matrix in which D, H and face pressure are varied independently so that a genuine diameter effect can be isolated. This study compares six static PLAXIS 3D cases using an explicit geometric definition: H is soil cover above the tunnel crown, D is excavation diameter, and H/D is their ratio. Crown-line surface settlement decreases with H/D within both diameter groups, from 4.48 to 2.49 mm for D = 4.3 m and from 6.05 to 1.54 mm for D = 6.8 m. The six cases do not support a universal independent diameter effect because absolute cover and prescribed face pressure vary with the geometry. The results should therefore be used as a bounded parametric comparison, not as a general diameter law or a continuous optimization. All converted maximum absolute ground strains remain below the Sakurai critical strain; however, this screen does not verify lining axial force, bending moment, shear, joint opening, or crack capacity. The equivalent continuous linear-elastic lining also cannot demonstrate yielding or flexible-joint behavior. The Peck cross-check gives 7.42% error at the centerline but 23.53% MAPE across the three reported points. This partial validation, together with the missing formal mesh and boundary sensitivity datasets, defines the limits of the conclusions and the requirements for future calibrated analyses.

REFERENCES

Ads, A., Islam, M. S., & Iskander, M. (2021). Effect of face losses and cover-to-diameter ratio on tunneling induced settlements in soft clay, using transparent soil models. Geotechnical and Geological Engineering, 39(8), 5529–5547. https://doi.org/10.1007/s10706-021-01843-7

Agarwal, J., & Sarkar, R. (2024). Greenfield settlements due to tunnelling using tunnel boring machine (TBM) in layered soils: A parametric study. Sādhanā, 49, Article 75. https://doi.org/10.1007/s12046-023-02425-4

Bentley Systems. (2024). PLAXIS 3D reference manual. Bentley Systems Inc. https://communities.bentley.com/products/geotech-analysis/w/wiki/46137/manuals---plaxis

Chakeri, H., Özçelik, Y., & Ünver, B. (2013). Effects of important factors on surface settlement prediction for metro tunnel excavated by EPB. Tunnelling and Underground Space Technology, 36, 14–23. https://doi.org/10.1016/j.tust.2013.02.002

Chakeri, H., & Ünver, B. (2014). A new equation for estimating the maximum surface settlement above tunnels excavated in soft ground. Environmental Earth Sciences, 71(7), 3195–3210.

https://doi.org/10.1007/s12665-013-2707-2

Fang, Q., Liu, X., Zeng, K., Zhang, X., Zhou, M., & Du, J. (2022). Centrifuge modelling of tunnelling below existing twin tunnels with different types of support. Underground Space, 7(6), 1125–1138. https://doi.org/10.1016/j.undsp.2022.02.007

Fargnoli, V., Boldini, D., & Amorosi, A. (2015). Twin tunnel excavation in coarse grained soils: Observations and numerical back-predictions under free field conditions and in presence of a surface structure. Tunnelling and Underground Space Technology, 49, 454–469. https://doi.org/10.1016/j.tust.2015.06.003

Hollmann, F. S., & Thewes, M. (2013). Assessment method for clay clogging and disintegration of fines in mechanised tunnelling. Tunnelling and Underground Space Technology, 37, 96–106. https://doi.org/10.1016/j.tust.2013.03.010

Kasper, T., & Meschke, G. (2006). On the influence of face pressure, grouting pressure and TBM design in soft ground tunnelling. Tunnelling and Underground Space Technology, 21(2), 160–171. https://doi.org/10.1016/j.tust.2005.06.006

Liu, C., Cui, J., Zhang, Z. X., Liu, H., Huang, X., & Zhang, C. Q. (2021). The role of TBM asymmetric tail-grouting on surface settlement in coarse-grained soils of urban area: Field tests and FEA modelling. Tunnelling and Underground Space Technology, 111, Article 103857. https://doi.org/10.1016/j.tust.2021.103857

Liu, Y., Liu, K., Li, X., & Yan, Z. (2024). Optimizing the support system of a shallow buried tunnel under unsymmetrical pressure. Buildings, 14(6), Article 1825. https://doi.org/10.3390/buildings14061825

Loganathan, N., & Poulos, H. G. (1998). Analytical prediction for tunneling-induced ground movements in clays. Journal of Geotechnical and Geoenvironmental Engineering, 124(9), 846–856. https://doi.org/10.1061/(ASCE)1090-0241(1998)124:9(846)

Mair, R. J., Taylor, R. N., & Bracegirdle, A. (1993). Subsurface settlement profiles above tunnels in clays. Géotechnique, 43(2), 315–320. https://doi.org/10.1680/geot.1993.43.2.315

Mánica, M. A., Simo, E., Gens, A., Herold, P., Nagel, T., Ovando, E., & Seidel, D. (2024). Numerical assessment of the time-dependent behaviour of a tunnel with a yielding support system for a potential repository in claystone. Geomechanics for Energy and the Environment, 39, Article 100578. https://doi.org/10.1016/j.gete.2024.100578

Mohyla, M., Vojtasik, K., Hrubesova, E., Stolarik, M., Nedoma, J., & Pinka, M. (2020). Approach for optimisation of tunnel lining design. Applied Sciences, 10(19), Article 6705. https://doi.org/10.3390/app10196705

O'Reilly, M. P., & New, B. M. (1982). Settlements above tunnels in the United Kingdom—Their magnitude and prediction. In Tunnelling '82 (pp. 173–181). Institution of Mining and Metallurgy.

Peck, R. B. (1969). Deep excavations and tunneling in soft ground. In Proceedings of the 7th International Conference on Soil Mechanics and Foundation Engineering, State-of-the-Art Volume (pp. 225–290). Sociedad Mexicana de Mecánica de Suelos.

Sagaseta, C. (1987). Analysis of undrained soil deformation due to ground loss. Géotechnique, 37(3), 301–320. https://doi.org/10.1680/geot.1987.37.3.301

Sakurai, S. (1997). Lessons learned from field measurements in tunnelling. Tunnelling and Underground Space Technology, 12(4), 453–460. https://doi.org/10.1016/S0886-7798(98)00004-2

Sass, I., & Burbaum, U. (2009). A method for assessing adhesion of clays to tunneling machines. Bulletin of Engineering Geology and the Environment, 68(1), 27–34. https://doi.org/10.1007/s10064-008-0178-6

Sharghi, M., Chakeri, H., & Özçelik, Y. (2017). Investigation into the effects of two component grout properties on surface settlements. Tunnelling and Underground Space Technology, 63, 205–216. https://doi.org/10.1016/j.tust.2017.01.004

Song, G., & Marshall, A. M. (2020). Centrifuge modelling of tunnelling induced ground displacements: Pressure and displacement control tunnels. Tunnelling and Underground Space Technology, 103, Article 103461. https://doi.org/10.1016/j.tust.2020.103461

Suárez-Fino, J. F., & Mayoral, J. M. (2024). Numerical modeling for tunnel lining optimization. Applied Sciences, 14(16), Article 7415. https://doi.org/10.3390/app14167415

Xie, X., Yang, Y., & Ji, M. (2016). Analysis of ground surface settlement induced by the construction of a large-diameter shield-driven tunnel in Shanghai, China. Tunnelling and Underground Space Technology, 51, 120–132. https://doi.org/10.1016/j.tust.2015.10.008

Zaheri, M., Ranjbarnia, M., Dias, D., & Oreste, P. (2020). Performance of segmental and shotcrete linings in shallow tunnels crossing a transverse strike-slip faulting. Transportation Geotechnics, 23, Article 100333. https://doi.org/10.1016/j.trgeo.2020.100333

COPYRIGHTS

©2023 The author(s). This is an open access article distributed under the terms of the Creative Commons Attribution (CC BY 4.0), which permits unrestricted use, distribution, and reproduction in any medium, as long as the original authors and source are cited. No permission is required from the authors or the publishers.

HOW TO CITE THIS ARTICLE

Moradi, G. & Jader Abdulhasan, N. (2026). Numerical Analysis of the Effect of the Soil-Cover-to-Excavation-Diameter Ratio on Surface Settlement and Ground-Strain Stability Screening of Shallow Tunnels in Clayey Soil Using PLAXIS 3D. (e743261). International Journal of Urban Management and Energy Sustainability, 7(3), e743261

DOI:10.22034/ijumes.2026.2108972.1425